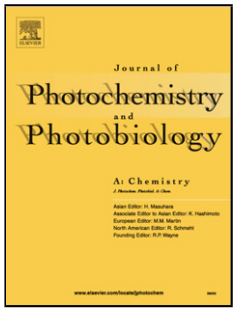

Title: Synthesis, physicochemical and spectroscopic characterizations of azochalcone derivative towards solar cells application

Author: M.M. Makhlouf A.S. Radwan M.R.E. Aly

PII: S1010-6030(16)30382-3
DOI: http://dx.doi.org/doi:10.1016/j.jphotochem.2016.09.025
Reference: JPC 10377

To appear in: *Journal of Photochemistry and Photobiology A: Chemistry*

Received date: 16-5-2016
Revised date: 21-9-2016
Accepted date: 23-9-2016

Please cite this article as: M.M.Makhlouf, A.S.Radwan, M.R.E.Aly, Synthesis, physicochemical and spectroscopic characterizations of azochalcone derivative towards solar cells application, Journal of Photochemistry and Photobiology A: Chemistry http://dx.doi.org/10.1016/j.jphotochem.2016.09.025

Synthesis, physicochemical and spectroscopic characterizations of azochalcone derivative towards solar cells application

M. M. Makhlouf [1,2,*], A. S. Radwan[3,4], M. R. E. Aly [5,6]

[1]Department of Physics, Faculty of Applied Medical Sciences, Taif University, 21995, Saudi Arabia.

[2]Department of Physics, Faculty of Science, Damietta University, 34517 New Damietta, Egypt.

[3]Department of Chemistry, Faculty of Applied Medical Sciences, Taif University, 21995, Saudi Arabia.

[4]Chemical and Environmental Affairs Sector, Ministry of Electricity and Energy, Ismailia, Egypt

[5]Department of Chemistry, Faculty of Science, Port Said University, Egypt

[6]Department of Chemistry, Faculty of Science, Taif University, 21995, Saudi Arabia.

Graphical Abstract

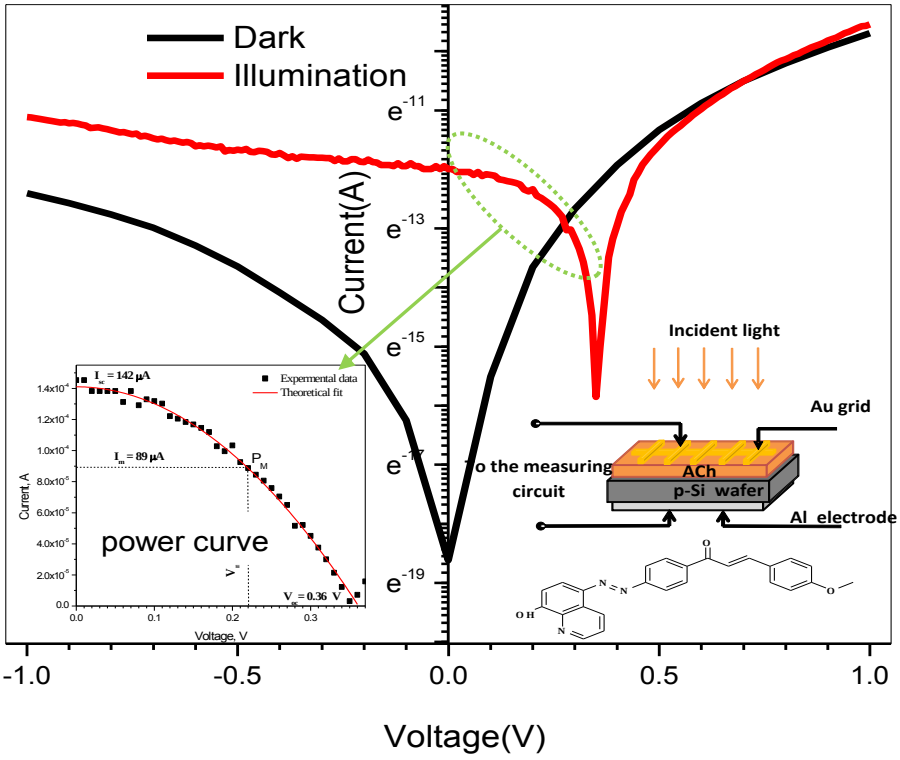

Highlights

- Novel azochalcone dye (**ACh**) was synthesized and characterized
- The structure analysis of **ACh** dye showed a nanocrystal structure based thin films.
- The optical constants and optical band gap of **ACh** dye thin films were calculated.
- Hybrid Au/**ACh**/p-Si/Al heterojunction solar cell was fabricated.
- Electronic transport and photovoltaic characterization of the solar cell were studied.

Abstract

A novel azochalcone derivative (**ACh**) has been synthesized by the reaction of azo-ketone and 4-anisaldehyde in ethanolic NaOH. The synthetized compound was characterized by FT-IR, ^{1}H NMR, and Mass spectra. Thin films with various thickness of **ACh** were deposited by thermal evaporation technique onto glass, quartz and Si wafer substrates under vacuum of 10^{-5} Torr. Structural analysis of these thin films was investigated by the field emission scanning electron microscopy (FE-SEM) and X-ray diffraction (XRD) patterns. The optical constants such as: refractive index (*n*), extinction coefficient (*k*) and optical band gap (E_g) of pristine and annealed films have been studied in the wavelength region 200–2500 nm. Analysis of the absorption coefficient, α, spectrum shows that the most probable transition is the indirect allowed transition. The onset and fundamental optical band gaps for **ACh** film are found to be 2.44 and 3.37 eV, respectively. The annealing temperature changes the optical constants. Tunable structural and optical properties of **ACh** open up the avenue to building up the solar cell based on **ACh**. The electronic transport mechanisms and photovoltaic properties of the fabricated solar cell of Au/**ACh**/p-Si/Al have been studied.

Keywords: Chalcones; Synthesis; Thin films; Optical properties; Electrical Mechanisms; Solar cells.

*Corresponding author: M.M. Makhlouf

Email: m_makhlouf@hotmail.com; m.makhlouf@edu.tu.sa

1. Introduction

Chalcones, as one of the well-known class of organic compounds which are mostly present in flavonoids [1]. Chemically, they are open chain of flavonoids consisting two aromatic rings having diverse array of substitutes linked by α, β-unsaturated carbonyl groups. Chalcones possess conjugated double bonds and a completely delocalized π-electron system on both benzene rings. Most of chalcones can be synthesized in laboratory by simple and inexpensive method depends on the condensation product of with aromatic aldehydes in the presence of strong base which is called Claisen-Schmidt reaction [2, 3]. Because of the ketovinylenic group (–CO–CH=CH-) and

π-conjugated bridges in chalcones and their analogs, they exhibit numerous chemical and physical properties, for instance optical and fluorescence properties [4, 5] and electric properties [6,7]. Chalcones have attracted much attention for several decades due to their potential technological application in fields of optical and photochemical sensors [8, 9], ultrafast optical nonlinearities [10], optical filters [11], optical switch [12], fluorescent probes [13] optical computing and optical communication [14, 15]. The structure-property relationships of 3,4,5-trimethoxy chalcone explored by Bing Gu et al. [16]; showed that the chalcone derivatives are highly promising in photovoltaic devices applications. The synthetic flexibility, a strong donor-acceptor intermolecular interaction and delocalized π-electrons system and lower dielectric constants are main features of chalcones [17]. Furthermore, chalcones have charge transfer character of the low-lying π-π^* transition from the phenyl ring to the polyene chain allows one to vary the energy of the intense transition introducing substituents in the phenyl ring [18]. Electronic structure of chalcone derivatives was explored mostly in their singlet π-π^* states in order to analyze the absorption spectra of substituted chalcones. Substituents in the phenyl ring conjugated with -C=C- group affect the absorption maximum with a greater extent than those in the phenyl ring conjugated with –C(=O)– group [18]. Both electron–donor (E-D) and electron–acceptor (E-A) substituents cause a decrease in the energy of the $S_{\pi\text{-}\pi^*}$-state. These promising features of chalcones allow the researchers to design new chalcone molecules substituted for donor or acceptor groups, which gives an understanding of structure-property relationship. Pyrrole-chalcone derivatives have been synthesized using chloro- and nitro-substituted aromatic aldehyde. The products were characterized by ^{1}H NMR, UV–Vis., FT-IR spectroscopic methods and quantum chemical calculations. The UV–Vis. spectra study reveals that the compounds are almost transparent and photosensitive in the visible region [19]. The chalcone-cyclophosphazene compounds containing dioxybiphenyl groups were synthesized by using of K_2CO_3/acetone system [20]. Komarova et al. [21] studied the solvent effect on the geometry and energies of the low-lying excited states of chalcone and its amino-derivatives using quantum chemical approach. The solvent

effect on the geometries and the energy shifts due to dipole–dipole interaction with the medium. The metal complexes based chalcones with metals (Cu, Ni, Co, Pt, Cd and Zn) possess a novel structure of interesting features and promising optical properties [22, 23].

Azo-coupling is one of the most important reactions for combining derivatives of aromatic rings and preparing azobenzene derivatives containing active functional groups as a precursor for further synthesis to give different organic molecules such as: azo-amide [24] and azo-imine [25]. Hence, based upon the promising properties of chalcones and azo compounds and in continuation for search for newer molecules for better properties an attempt has been made to synthesize azochalcone derivative (**ACh**) and screening for its physicochemical features. Herein, we report a simple method [2, 3] to synthesize azochalcone derivative from the corresponding aldehyde and ketone using Aldol condensation. The produced **ACh** was investigated by studying spectroscopic and physicochemical features.

Keeping in view the importance of thin film technology that plays an important role in the high-tech applications such as: nano- and micro-electronics, optoelectronics, photovoltaic devices and dye-sensitized solar cells (DSSCs), we have decided to prepare the thin films of **ACh** using the thermal evaporation technique and study the structural, optical and electrical properties of these films. Furthermore, the hybrid heterojunction solar cell based **ACh**/p-Si has been fabricated. The electrical transport mechanisms of this cell were studied and its photovoltaic parameters were evaluated.

2. Experimental details

2.1. Syntheses of azochalcone derivative, (E)-1-(4-((E)-(8-hydroxyquinolin-5-yl) diazenyl)phenyl)-3-(4-methoxyphenyl)prop-2-en-1-one, (**ACh**).

Step 1: A solution of aryl diazonium salt was prepared by adding $NaNO_2$ (0.01 mol, 10 ml H_2O) to cold solution of 4-aminoacetophenone (0.01 mol,) in 3 ml conc. HCl with stirring. The

freshly prepared solution was added with continuous stirring to cold solution of 8-hydroxyquinoline (0.01 mol, 1.45 g) in NaOH (30%, 10 ml). The reaction mixture was stirred at 0-5 °C for 2 h, diluted with water, and then neutralized by dil. HCl. The dark red precipitate was filtered, washed thoroughly with H_2O until neutral to litmus paper then dried well. Upon recrystallization from EtOH, intermediate azodye **3** [26] was obtained as in (74 %) yield.

Step 2: A mixture of 4-methoxy benzaldehyde (1.36 g, 0.01mol), intermediate **3** (2.91 g, 0.01mol) and NaOH (1.2 g, 0.03mol) in EtOH (20 ml) was stirred at ambient temperature overnight. The reaction mixture was neutralized with AcOH and the brown precipitate was filtered at the pump, washed thoroughly with H_2O and dried well. Recrystallization from EtOH afforded conjugate **ACh** as fine brown yield (68%); m.p. 255 - 258 °C; IR (ύ, cm^{-1}): 3450–3163 ($O–H_{str.}$), 3059 ($=C–H_{str.}$), 2839 ($CH_{3str.}$), 1675,1654 ($C=O_{str.}$,), 1598, 1568, 1503 ($C=N_{str.}$, $C=C_{str.}$, $N=N_{str.}$), 1200 (Ar $C–O_{str.}$), 1023 ($CH_3–O_{str.}$), 808, 782 ($Ar–H_{def}$); ^{1}H NMR (400 MHz, DMSO–d_6): δ 9.11 (s, 1H, Ar), 8.56 (s, 1H, Ar), 8.15 (d, 1H, *J* 8.4 Hz, Ar), 8.14–7.70 (m, 7H, COCH=C*H*, 6 H–Ar), 7.68 (d, 1H, $J_{\alpha,\beta}$ 15.6 Hz, COC*H*=CH), 7.47 (s, 1H, Ar), 7.12 (d, 1H, *J* 9.2 Hz, Ar), 7.02 (d, 1H, *J* 8.8 Hz, Ar), 6.41 (s, 1H, ~~Ar~~ OH), 3.82 (s, 3H, OCH_3); EI–MS (*m/z*, %): 409 (M+, 38), 294 (16), 251 (11), 250 (70), 205 (30), 204 (100). $C_{25}H_{19}N_3O_3$ (409.44)

2.2. Thin films preparation

The **ACh** dye was flashed through column chromatography of silica gel (Baker, 30–60 µm) for more purification. The homogeneous thin films of **ACh** were thermally prepared by a conventional thermal evaporation technique (Edward Coating Unit E-306) onto pre-clean flat glass, quartz and Si wafer substrates for structural, optical, electrical measurements, respectively, at room temperature under pressure of 10^{-5} Torr. **ACh** was sublimated using quartz crucible that was subjected to induction heating from molybdenum heater boat. The thickness of the films was

measured by using a quartz crystal monitor (Maxtek. Inc., TM-350, USA) controls the rate of deposition (2.5 Å/s) and film thickness (140 nm) for structural and optical measurements.

2.3 Fabrication of solar cell

The thin film of **ACh** with a thickness of about 90 nm was deposited on the front surface of p-Si wafer substrate and then the layer of **ACh** was over coated by a mesh Au electrode was deposited through a special mask on the surface of the organic thin film. The back side of Si was coated by a thick layer of Al electrode. Au and Al electrodes were thermally evaporated directly from basket-shaped tungsten filaments. Thus, an Au/**ACh**/p-Si/Al heterojunction solar cell was designed. The effective area of the solar cell is 0.12 cm^2. The annealing temperature of the fabricated heterojunction at 373 K for 2 hours is needed to enhance the performance of the junction.

3.4. Measurements

Melting points were determined on Electrothermal apparatus and are uncorrected. Flash chromatography was carried out on silica gel (Baker, 30–60 µm). TLC Monitoring tests were carried out using eluent (tolune: acetone: isopropanol) (2: 2: 1), plastic sheets precoated with silica gel 60 F_{245} (layer thickness 0.2 mm) purchased from Merck. Spots were visualized by their fluorescence under UV–lamp (λ 245 and 366 nm). NMR spectra were recorded on Bruker 400 MHz spectrometers. IR–spectra were recorded on ATR–Alpha FT–IR Spectrophotometer from 400 to 4000 cm^{-1}. Shimadzu GCMS-QP-1000EX mass spectrometers at 70 eV. Analysis of X-ray Diffraction (XRD) pattern for the powder and thin films of **ACh** were performed at room temperature by using Philips X-ray diffraction system (model $X^{/}$ Pert Pro.) with utilized monochromatic CuK_α radiation of λ=1.5418 Å. The structural morphology of the pristine and annealed thin films of **ACh** were investigated using field emission scanning electron microscope, FE-SEM, (model FEI QUANTA 250 FEG) after coating films with thin layer of Au.

A JASCO (V-570 UV-VIS-NIR) double-beam spectrophotometer is used for measuring The transmittance, *T(λ)*, and reflectance, *R(λ)*, spectra of the films. The *T*(λ) and *R*(λ) were measured as a function of wavelength of the incidence of light in the spectral range 200 - 2500 nm.

The electrical and photovoltaic properties of the heterojunction device were investigated by *I–V* measurements using source-meter (Keithly type 2635A). The measurements were carried out at in dark / light conditions. The intensity of incident light from tungsten filament lamp was recorded by a calibrated digital light meter (Lutron-Model LX-107) situated at the same level position of the device and is calculated as 100 W/m^2.

3. Results and discussion

3.1. Chemical characterization

The target **ACh** dye was prepared by modular synthesis starting with 8-hydroxychinoline **1** and *p*-Aminoacetophenone **2**. Thus, diazotization of compound **2** with $NaNO_2$/HCl followed by coupling with compound **1** afforded smoothly the intermediate acetylated azodye derivative **3**. Taking the advantage of the acetyl tag in compound **2**, Claisen–Schmidt condensation was easily performed at ambient temperature in the presence of 3.0 equivalents of NaOH to afford conjugate ACh in 68% yield (Scheme 1).

The FT-IR spectrum of **ACh** compound (Fig. S1 in Supplementary material) displayed a broad O–H stretching vibration band at 3400–3160 cm^{-1}. The band at 3059 cm^{-1} refer to aromatic and olefinic C–H stretching vibrations, while that at 2838 cm^{-1} is for symmetric vibrations of C–H bonds in the CH_3 group. The stretching vibration of the C=O bond was observed at 1675 cm^{-1}. This expected bathochromic shift is attributed to conjugation of the group with π–cloud of the benzene ring and the olefinic linkage. The weak band at 1675 cm^{-1} is attributed to overtone of the C=O stretching band with the C–H bending modes that is known as Fermi resonance. The bands at 1598,

1568 and 1503 cm^{-1} could not be clearly assigned but they are related to the stretching vibrations of the C=N, C=C and N=N bonds. The Ar–O stretching band was noticed at 1200 cm^{-1}, while the O–CH_3 band was normally observed at 1023 cm^{-1}. The hypsochromic shift of the first band is related to strengthening of the Ar–O linkage by the *+M* effect of the etheric oxygen. Despite the two aryl groups in the molecule are *p*-substituted, two out-of-plane Ar–H bending bands were observed at 808 and 782 cm^{-1} due to the two groups.

In the ^{1}H NMR spectrum of **ACh** compound as shown in Fig. S2 in Supplementary material, the CH_3 group was observed as a singlet at δ 3.82 ppm. The O–H signal was assigned as singlet at δ 6.41 ppm and this signal disappeared by deuteration. Other protons were observed in the aromatic range. Both signals were a good evidence for the progressing of Claisen–Schmidt condensation. In addition, the doublet δ 7.68 ppm with a large coupling $J_{\alpha,\beta}$ 15.6 Hz is another proof of this reaction and it is attributed to the α-carbon that is less deshielded than the β–carbon of the olefinic linkage. This high coupling confirms the *trans*–orientation about the olefinic group. The EI-MS of **ACh** compound (Fig. S3 in Supplementary material) displayed a molecular ion peak at *m/z* 409 that matches the calculated mass for the molecular formula of the molecule ($C_{25}H_{19}N_3O_3$). This peak was one-third as intense as the base one at *m/z* 204. Despite, the major peaks could not be interpreted by common fragmentation mechanisms of chalcones and azo-dyes, it seems that the fragmentation mode shown in (Scheme 2) explains the peak at *m/z* 251.

3.2 Structural properties:

The structure analysis was carried out using XRD and FESEM for pristine and annealed **ACh** thin films on the glass substrates. Fig. 1(a) shows the XRD pattern of as-synthetized powder form of **ACh**; It was noted that, XRD pattern has many diffraction peaks with different intensities which indicates that, it has a polycrystalline structure. The broad halo in the diffraction pattern is due to amorphous character is evidenced by the XRD pattern for pristine and annealed **ACh** thin films as

shown in Fig. 1(b). A small single peak as observed around ($2\theta = 39.3^{o}$) can be attributed to the nanocrystallite structure of annealed thin film as shown in Fig. 1(c).

The FE-SEM investigation reveals the formation of films with different topographies. Fig. 2 displays FE-SEM images of pristine and annealed **ACh** thin films. As seen in Fig. 2(a), the morphology of a pristine film is characteristic of an amorphous structure and this character is evidenced by the XRD pattern as seen in Fig. 1(b). Fig. 2(b) shows the structure of thermally annealed **ACh** film that contains nanocrystals distributed uniformly over the image, which is consistent with the result of XRD technique and confirmed that the structure of annealed film of **ACh** is nanocrystallites dispersed in amorphous matrix structure.

3.3 Optical properties

Analysis of the absorption spectra of the semiconductor materials can be used for the investigation of the important factors such as: determining the light-harvesting capacity, the type of most probable electronic transitions and the value of the optical energy band gap for these materials. Fig.3 shows the absorption spectrum for the pristine and annealed **ACh** thin films as a function of the wavelength in the UV-Vis. spectral region from 200 to 700 nm. The absorption spectrum exhibits two transition bands that can be attributed to the orbital molecular transition from bonding to antibonding molecular orbital. The absorption bands of **ACh** depend on aromatic rings, C=C of chalcone and azo functional group. The absorption band due to azo group is located in the visible region of spectra as absorption peak at 382 nm, which is ascribed to the $n \rightarrow \pi^{*}$ transition. The chalcone group and aromatic rings have absorption peak at 241 nm in UV. region and this band is ascribed to the absorption of the $\pi \rightarrow \pi^{*}$ transition. Annealing temperature at 473 K decreases the value of the absorption over the spectral range of UV-Vis. region.

The transmittance, $T(\lambda)$, and the reflectance, $R(\lambda)$, spectra are measured in the wavelength ranged from 200 to 2500 nm of pristine and annealed **ACh** thin films are depicted in Fig.4. The $T(\lambda)$ and $R(\lambda)$ spectra can be divided into two regions depending on the wavelength of incident photons,

λ: region I at shorter wavelengths, ($\lambda < 680$ nm); the total sum of $T(\lambda)$ and $R(\lambda)$ is less than unity due to absorption spectrum, this means there is no light transmitted out the **ACh** films and all photons of incident light in this region almost absorbed. These films are considered to be a good absorbers for light in UV spectrum, where minimum and maximum percentage values of $T(\lambda)$ and $R(\lambda)$ are 0 – 11%, and 0 – 5%, respectively; for the pristine **ACh** film. Therefore, this film might be used as an optical filter in the limited range of spectrum. Region II, at longer wavelengths ($\lambda > 680$ nm), no absorption takes place and the percentage of $T(\lambda)$ ($\geq 92\%$) is very greater than the percentage of $R(\lambda)$ ($\leq 8\%$) and their total sum approaches unity ($T(\lambda) + R(\lambda) \approx 1$). In this region, the films are transparent for the light and the value of absorption spectrum approaches to zero. Therefore, in that transparent region; we can calculate the values of refractive index, absorption coefficient and dispersion parameters for these films. Annealing **ACh** films at 473 K increases the values of $T(\lambda)$ and $R(\lambda)$ spectra and shifts the transmittance edge to the low wavelengths side which reflects in the variation of the value of the optical energy band gap.

The complex refractive index, n^*, of the films can be expressed in terms of real part as a refractive index, n, and imaginary part as an extinction coefficient, k, where $n^* = n + ik$. The n is related to the optical dispersion parameters, while k provides a measure of dissipation rate of the electromagnetic wave in the dielectric medium.

The values of refractive index, n, and the extinction coefficient, k, of **ACh** films deposited onto thick non-absorbing quartz substrates can be computed by using the absolute values of T and R. These absolute values are calculated according to the method reported in previous works [27, 28]. The calculated values of refractive index, n, and the extinction coefficient, k, were computed by a program comprising a modified bi-variant search technique [29 - 31] based on Murmann's exact equations [30, 31] and satisfy the solving of minimizing $|\Delta T|^2$ and $|\Delta R|^2$ simultaneously, where

$$|\Delta T|^2 = \left|T_{cal}(n,k,d,\lambda) - T_{\exp}\right|^2 \approx o \qquad (1.a)$$

and

$$|\Delta R|^2 = |R_{cal}(n,k,d,\lambda) - R_{\exp}|^2 \approx o \quad (1.b)$$

where T_{cal} and R_{cal} are the calculated values of transmittance and reflectance using Murmann's exact equations, $T_{\exp}$ and $R_{\exp}$ are the experimental values of transmittance and reflectance, respectively; and d is the thickness of film. The spectral behavior of n for pristine and annealed **ACh** thin films is illustrated in Fig. 5(a). It shows an anomalous dispersion in the range from 190 to 860 nm with two dispersion peaks for **ACh** films; however, it can be explained according to multi-oscillator model [31]. The spectrum of n shows a normal dispersion behavior in wavelength ranged 750 - 2500 nm and can be explained by applying the Wemple-DiDomenico model [32, 33]. Fig. 5(b) shows the spectral behavior of k for the pristine and annealed **ACh** thin films as a function of wavelength in UV-Vis-NIR regions of spectra. The k spectrum has two peaks around 230 - 470 nm. Annealing temperature decreases the value of the refractive and absorption indices all over the spectra for **ACh** thin film is due to decreasing of the aggregation of azochalcone molecules in these films.

The absorption coefficient, α, is related to k through the relation: $\alpha = 4\pi k/\lambda$. The spectral distribution of α for pristine and annealed **ACh** thin films as a function of wavelength of the incident light are depicted in Fig.6. These films show high value of absorption spectra ($\alpha > 10^5$ cm^{-1}) which are in the UV-Vis region of incident light. Annealing temperature decreases the value of α and shifts the absorption edge toward high photon energy side of spectra. Analysis of the absorption spectrum edge is well-known method for determining the type of the transitions and also gives information about the values of optical energy gap, E_g, of different crystalline and amorphous materials. Tauc [34, 35] assumed that the relation between α and incident photon energy, $h\nu$, for most amorphous semiconductors through the following general relation:

$$\alpha h\nu = B(h\nu - E_g)^r \quad (2)$$

Where B is a constant related to the electrical conductivity and energy level separation and r is a number that characterize the type of transition. r = 2 or 3 for indirect allowed and forbidden

transitions, respectively; exhibit in most amorphous semiconductors and r = 1/2 or 3/2 for direct allowed and forbidden transitions, respectively; exhibit in most crystalline semiconductors. The relation between $(\alpha h\nu)^{1/2}$ versus photon energy, $h\nu$, is found to be the best fitting of results for a pristine and annealed **ACh** thin films at r = 2, this means the most probable type of electron transition is indirect allowed transition as illustrated in Fig.7. The value of E_g can be calculated by extrapolating the linear portion of the plot to intercept the abscissa axis in the value of energy gap. The values of E_g for pristine film are 2.44 and 3.37 eV for onset and optical band gap, respectively. Annealing temperature decreases the onset and optical band gap to be 2.28 and 3.07 eV, respectively. This decreasing in energy gaps is due to the creation of new impurity or the extension of the localized state inside the band gap. It should be noted that the values of optical band gap obtained in the present work are consistent with the values reported in the literatures [17, 36]. The value of optical band gap of ACh thin films is closely matched with the optical band gap of value 2.31 eV for mono-chalcone [17] and 3.05 eV for DPMS chalcone derivative [36].

3.3. Characteristics of azochalcone / p-Si heterojunction solar cell

3.3.1 Electric transport mechanism in forward bias direction of heterojunction solar cell

Fig. 8 shows the semi-logarithmic current-voltage (I-V) characteristics of Au/**ACh**/p-Si/Al heterojunction solar cell in dark and under illumination at ambient temperature. For I-V characteristics in dark condition, it observed that, this device exhibits a rectifying behavior due to the injection of the charge carriers from electrode to **ACh** layer. Under low forward voltage bias ($0 < V < 0.4$ volt), the logarithmic current, log I, increases linearly with the voltage bias, V, until reaching a certain value, and then it increases exponentially with applied high voltage bias ($0.4 \leq V \leq 1$ volt). On the other hand, the log I is very small under the reverse voltage bias, and this behavior can be understood in terms of the change of width of depletion region for the diode behavior [37]. This nonlinearity behavior is due to the effect of series resistance, R_s, and the interface states when the applied voltage is sufficiently large. The R_s is important parameter for downward curvature of the

forward I-V characteristics. On the other side, an ideal device requires the higher shunt resistance, R_{sh}, which plays an important role in the values of reverse I-V characteristics. The R_s and R_{sh} can be calculated by the method was stated in previous report [38]. It is showed that, R_s and R_{sh} were found to be 13.4 kΩ and 1.12 MΩ, respectively. The heterojunction has high R_s value due to the amorphous interface layer in that junction [39].

In order to determine conduction mechanism of Au/**ACh**/p-Si/Al heterojunction, the different conduction mechanisms were tested. For lower voltage (0< V< 0.4 volt), we invoke the thermionic emission model for investigating the conduction mechanism of that device. According to this model, the current can be expressed as [40, 41]

$$I = I_O \exp\left(\frac{qV}{nK_BT}\right)\left[1-\exp\left(-\frac{qV}{nK_BT}\right)\right] \quad (3)$$

where I_O is the saturation current, K_B is the Boltzmann constant, T is the absolute temperature, q is the charge of electron, V is the applied voltage and n is the ideality factor. The saturation current, $I_{O,}$ is given by

$$I_O = AA^*T^2 \exp\left(-\frac{q\varphi}{K_BT}\right) \quad (4)$$

Where A is the active area of the device, A^* is effective Ridchardson constant (A^* = 32 for p-Si) and φ is the zero-bias barrier height. The value of n can be calculated from the slope of linear relation between log I and V (lower voltage region) as shown in Fig. 8. It was found to be 1.75 which is higher that the ideality value of 1.02 [42] and that may due to the presence of interfacial native oxide layer on silicon substrate, series resistance and barrier height inhomogeneity [43]. The formation of such a thin interfacial oxide layer is inevitable during the fabrication of the solar cell by the thermal evaporation technique and before evaporation of **ACh** compound on the front surface of the p-type Si substrate [42, 43]. On the other hand, the value of φ can be obtained from Eq. (4) and was found to be 0.81 eV. At relatively higher voltage bias (0.4 ≤ V ≤ 0.1 volt), in order to determine the

conduction mechanism that control the device characteristic in that voltage range, the relation current and voltage in I-V characteristic should be plotted in logarithmic scale and according to the power law of $I = V^m$ where m is the slope of graph log V- log I which is the dioristic value to recognize the type of conduction mechanism. Fig. 9 shows the linear relationship between log V and log I and its slope (m = 2.35) indicating that the space charge limited conduction (SCLC) mechanism is dominated [44].

3.3.2 Electric transport mechanism in reverse bias direction of heterojunction solar cell

Fig. 8 shows that the reverse current of the device is small compared with the forward current; this is due to that the current in reverse direction can be governed by current limitation mechanism. The dominated mechanism was found as Schottky effect [45]. The reverse current, I_{re}, can be explained in terms of the charge transport for this conduction mechanism as follows [45, 46]:

$$I_{re} = I_s \exp\left(\frac{\beta_s}{K_B T} \sqrt{\frac{V}{d}} \right) \tag{5}$$

where I_s is a constant, V is the applied voltage and d is the thickness of the film and β_s is the Schottky constant which can be theoretically calculated by the following relation,

$$\beta_s = \sqrt{\frac{e^3}{4\pi\varepsilon\varepsilon_o}} \tag{6}$$

ε and ε_o are the dielectric constant of the material and vacuum, respectively. From optical study, the value of ε is 4.76. The relation between log I_{re} and $V^{1/2}$ is depicted in Fig. 10. The slope of this linear relation can be used to calculate β_s, experimentally and it was found as 9.5 x 10^{-6} eV $m^{1/2}$ $V^{-1/2}$, while the theoretical value of β_s can be deduced from Eq.(6) and its value was found to be 1.2 x 10^{-5} eV $m^{1/2}$ $V^{-1/2}$. It is observed that, the experimental value of β_s is closer to the theoretical one and this support that the charge transport mechanism through device is the Schottky mechanism when the applied voltage is reverse bias.

3.3.3 Photovoltaic properties of the solar cell

The I-V characteristic of Au/**ACh**/p-Si/Al heterojunction solar cell under white light illumination of halogen lamp of power intensity of 100 mW/m^2 is shown in Fig. 8. It can be observed that there is a significant enhancement in the reverse current by the photo-illumination. This photosensitive property indicates that the device has the photovoltaic behavior. The light was harvested by the device and creates excitons in the **ACh** layer and electron-hole pairs in the Si waver. These excitons are dissociated into electron-hole pairs at the **ACh**/Si interface. In the presence of external applied electrical field, the electrons are transported in the Si and controlled by the Al electrode and leave holes was accelerated toward the Au electrode along the potential barrier at the interface. The total current of the device under illumination can be described by adding the photo-generated current to the dark current through the device.

The power curve for the device can be obtained by varying the load resistance from 0 to infinity at constant intensity of illumination light as shown in Fig. 11. The maximum power that can be extracted at the point for which the largest rectangle inscribed into the I-V power curve. It can be deduced from Fig. 11 many of photovoltaic parameters such as: the short circuit current, I_{sc}, of 142 μA and the open circuit voltage, V_{oc}, of 0.36 volt. The fill factor, *FF*, can be calculated from the relation [47, 48]:

$$FF = \frac{V_M I_M}{V_{oc} I_{sc}} \tag{7}$$

where V_M and I_M are the voltage and current at the maximum power point, respectively. *FF* is found to be 0.38. Furthermore, the electrical conversion efficiency, η, is calculated from the relation [47, 48]:

$$\eta = FF \frac{V_{oc} I_{sc}}{P_{in} A} \times 100\% \tag{8}$$

where *A* is the active area of the device and P_{in} is the intensity of incident light. The conversion efficiency of the fabricated Au/**ACh**/p-Si/Al heterojunction solar cell was calculated as 1.8 %.

Conclusion

A new azochalcone derivative (**ACh**) was synthesized and its characterization properties were investigated by FT-IR, ^{1}H NMR, and Mass spectra. The thin films of **ACh** were prepared by thermal evaporation technique at room temperature. Structural properties of **ACh** thin films have been investigated. The XRD for **ACh** in a powder form was a polycrystalline nature. The FE-SEM and XRD pattern showed the existence of amorphous structure of pristine thin film while, they reveal the nanostructure of the annealed thin film.

The optical properties of pristine and annealed **ACh** thin films were studied using spectrophotometric measurements of the transmittance and reflectance in the wavelength region 200–2500 nm, from which some optical constants such as the refractive index (n), extinction coefficient (k) and optical band gap (E_g) of the pristine and annealed films were determined.

The results of the optical absorption data showed that **ACh** thin films have mainly indirect onset and optical energy band gaps are found to be 2.44 and 3.37 eV, respectively and annealing temperature decreases these energy gaps to be 2.28 and 3.07 eV, respectively.

The results of this study indicate that **ACh** thin film as an organic semiconductor is a good candidate for optoelectronic devices based on its optical band gap and optical absorption spectrum. The **ACh** film is used to fabricate hybrid organic/inorganic heterojunction solar cell with a simple structure of Au/**ACh**/p-Si/Al. The electrical characteristics of the solar cell have been studied by current-voltage (I-V) in dark and under illumination at room temperature. The electric conduction mechanisms are governed by thermionic emission and space-charge-limited current (SCLC) for low and high applied bias, respectively. The photovoltaic parameters of the cell were calculated, the solar cell displays a fill factor of 0.38 and a power conversion efficiency of 1.8% under illumination.

References

[1] S. K. Awasthi, N. Mishra, B. Kumar, M. Sharma, A. Bhattacharya, LC Mishra, VK Bhasin, "Potent antimalarial activity of newly synthesized substituted chalcone analogs in vitro" Med. Chem. Res. **18** (2009) 407-420.

[2] D. Dive, C. Biot, "Ferrocene Conjugates of Chloroquine and other Antimalarials: the Development of Ferroquine, a New Antimalarial " Chem. Med. Chem. **3** (2008) 383- 391.

[3] D. Hwang, J. Huyn, G. Jo, D. Koh, Y. Lim, "Synthesis and complete assignment of NMR data of 20 chalcones" Magn. Reson. Chem. **49** (2011) 41-45.

[4] A. M. Asiri, ,S. A. Khana, H. M. Basisi "Single X- ray crystal and spectroscopic investigation of novel biologically active donor–acceptor chalcones as specific application for opto-electronics and photonics" J. Taiwan Inst. Chem. E. **59** (2016) 457-464

[5] C.G. Niu, A.L. Guan, G.M. Zeng, Y.G. Liu, Z.W. Li, "Fluorescence water sensor based on covalent immobilization of chalcone derivative" Anal. Chim. Acta **577** (2006) 264-270.

[6] V.S. Pandey, R. Dhar, A.K. Singh, A.S. Achalkumar, C.V. Yelamaggad, "Thermodynamic and electrical characteristics of the twisted grain boundary phases of 4-*n*-dodecyloxy-4′-(cholesteryloxycarbonyl-1-butyloxy) chalcone" Phase Transitions **83** (2010) 1049 -1058.

[7] E.D. D'silva, D.N. Rao, R. Philip, R.J. Butcher, Rajnikant, S.M. Dharmaprakash, "Synthesis, growth and characterization of novel second harmonic nonlinear chalcone crysta" J. Phys. Chem. Solids **72** (2011) 824-830.

[8] D. Millan, M. Dominguez, M.C. Rezende, "Solvatochromic hydrazone anions derived from chalcones" Dyes Pigments **77** (2008) 441- 445.

[9] Y. Wei, G. Qin, W. Wang, W. Bian, S. Shuang, C. Dong, "Development of fluorescent Fe(III) sensor based on chalcone" J. Lumin. **131** (8) (2011) 1672-1676.

[10] B. Gu, W. Ji, P.S. Patil, S.M. Dharmaprakash, "Raman study on the effects of sintering temperature on the $J_c(H)$ performance of MgB_2 superconductor" J. Appl. Phys. **103** (2008) 103511-103516.

[11] L. Mager, C. Melzer, M. Barzoukas, A. Fort, S. Mery, J.F. Nicoud, "High net gain at 514 nm in a photorefractive polymer doped with a chalcone derivative"Appl. Phys. Lett. **71** (1997) 2248–2250.

[12] M. P. Cockerham, C.C. Frazier, S. Guha, E.A. Chauchard, "Second-harmonic generation in derivatives and analogs of benzophenone and chalcone" Appl. Phys. B **53** (1991) 275–278.

[13] H.G.O. Alvim, E.L. Fagg, A.L. de Oliveira, H.C.B. de Oliveira, S.M. Freitas, M. A.E. Xavier, T.A. Soares, A.F. Gomes, F.C. Gozzo, W.A. Silva, B.A.D. Neto, "Probing deep into the interaction of a fluorescent chalcone derivative and bovine serum albumin (BSA): an experimental and computational study", Org. Biomol. Chem. **11** (29) (2013) 4764-4777

[14] H. Forejtnikova, K. Lunerova, R. Kubinova, D. Jankovska, R. Marek, R. Kareš, V. Suchy´ , J. Vondráček, M. Machala, "Chemoprotective and toxic potentials of synthetic and natural chalcones and dihydrochalcones in vitro" Toxicology **208** (2005) 81-93.

[15] Y. Xue, Y. Liu, L. An, L. Zhang, Y. Yuan, Jie Mou, L. Liu, Y. Zheng, "Electronic structures and spectra of quinoline chalcones: DFT and TDDFT-PCM investigation" Comp. Theor. Chem. **965** (2011) 146–153.

[16] Bing Gu, Wei Ji, P. S. Patil, S. M. Dharmaprakash, "Ultrafast optical nonlinearities and figures of merit in acceptor-substituted 3,4,5-trimethoxy chalcone derivatives: Structure-property relationships"J Appl Phys, **103**, (2008)103511- 5.

[17] A. M. Asiri, S. A. Khan, "Synthesis, characterization and optical properties of mono- and bis-chalcone" Mater. Lett. **65** (2011) 1749–1752

[18] Y. Xue, J. Mou, Y. Liu, X. Gong, Y. Yang, L. An, An ab initio simulation of the uv/visible spectra of substituted chalcones, Cent. Eur. J. Chem. **8** (2010) 928–936.

[19] R.N. Singh, Poonam Rawat, Vikas Baboo, Yashvinder Kumar, Spectroscopic and quantum chemical correlation for structural evaluation, chemical reactivity and non-linear optical property investigation of two chalcone having pyrrole moiety: A comparative study, J. Mol. Struct. **1085** (2015) 258 - 267.

[20] A. O. Gürgülü , K. Koran , F. özen, S. Tekin , S. Sandal, "Synthesis, structural characterization and anti-carcinogenic activity of new cyclotriphosphazenes containing dioxybiphenyl and chalcone groups" J. Mol. Struct. **1087** (2015) 1–10

[21] K.G. Komarova, S.N. Sakipov , V.G. Plotnikov , M.V. Alfimov "Luminescent properties of chalcone and its aminoderivatives" J. Lumin. **164** (2015) 57–63

[22] W. E. Rudzinski, T. M. Aminabhavi, N. S. Biradar, C. S. Patil "Tellurium complexes with substituted chalcones" Inorg. Chim. Acta **70** (1983) 175 - 178.

[23] BK. Sarojini, B. Narayana, B.V. Ashalatha, J. Indira, KG. Loba "Synthesis, crystal growth and studies on non-linear optical property of new chalcones" J. Cryst Growth **295** (2006) 54–59.

[24] J. P. LI, P. Liu, Y. L . Wang "An Efficient Method for the Synthesis of Acyl-diazenes Using $NaNO_2/NaHSO_4 \cdot H_2O$" Chin. Chem. Lett. **14** (7) (2003) 677 – 680.

[25] A. A. Jarrahpour, M. Motamedifar, K. Pakshir, N. Hadi, M. Zarei "Synthesis of Novel Azo Schiff Bases and Their Antibacterial and Antifungal Activities" Molecules 9 (2004) 815 – 824.

[26] Aytül Saylam, Zeynel Seferoğlu, Nermin Ertan, "Azo-8-hydroxyquinoline dyes: The synthesis, characterizations and determination of tautomeric properties of some new phenyl- and heteroarylazo-8-hydroxyquinolines", J. Mol. Liq. **195,** (2014) 267-276

[27] M. M. El-Nahass, A.A. Atta, H.E.A. El-Sayed, E. M. F EL-Zaidia " Structural and optical properties of Thermal evaporated magnesium phthalocyanine (MgPc) thin films. Appl Surf Sci 254(2008) 2458 - 2465.

[28] A.S. Radwan, M.M. Makhlouf , E. Abdel-Latif "Azothiophene dyes nanotubes structure based thin films: Synthesis, structural and optical characterization toward application in dye-sensitized solar cells" Dyes Pigments 134 (2016) 516 - 525.

[29] I. Konstantinov, T. Babeva, s. Kitova "Analysis of errors in thin-film optical parameters derived from spectrophotometric measurements at normal light incidence" Appl. Opt. **37** (1998) 4260 - 4267

[30] H. M. Liddeli, Computer-Aided Technique for the Design of Multilayer Filters, Hilger, Bristol, 1981.

[31] O. S. Heavens, G. Hass, R. Thus (Eds.), Physics of Thin Films, Academic press, New York, 1964, p. 193.

[32] S. H. Wemple, M. DiDomenico, "Optical Dispersion and the Structure of Solids" Phys. Rev. Lett. **23** (1969) 1156 - 1160.

[33] S.H. Wemple, M. DiDomenico "Behavior of the electronic dielectric constant in covalent and ionic materials" Phys. Rev. B **3** (1971) 1338 - 13351.

[34] J. Tauc, Amorphous and Liquid Semiconductors, Plenum Press, New York, 1974.

[35] E. A. Davis, N. F. Mott "Conduction in non-crystalline systems V. Conductivity, optical absorption and photoconductivity in amorphous semiconductors" Phil. Mag. **22** (197) (1970) 903 - 922.

[36] T.C.S. Shetty, S. Raghavedra, C.S.C. Kumar, S.M. Dharmaprakash, "Nonlinear absorption, optical limiting behavior and structural study of a new chalcone derivative-1-(3, 4-dimethylphenyl)-3-[4(methylsulfanyl) phenyl] prop-2-en-1-one" Opt. Laser Technol. **77** (2016) 23-30.

[37] H. S. Soliman, A.A. M. Farag, N. M. Khosifan, T.S. Solami, "Electronic and photovoltaic properties of Au/pyronine G(Y)/p-GaAs/Au:Zn heterojunction" J. Alloy Compd 530 (2015) 157-163.

[38] A. Ashery, G. Said, W.A. Arafa, A.E.H. Gaballah, A.A.M. Farag, "Structural and optical characteristics of PEDOT/n-Si heterojunction diode" Synthetic Met. **214** (2016) 92–99.

[39] B. Tatar, D. Demiroğlu, M. Urgen "Structure and photovoltaic properties of Ag/p-CuPc/a-Si/c-Si/Ag organic - inorganic hybrid heterojunction fabricated by chemical spray pyrolysis technique" Microelectron. Eng. **108** (2013) 150-157.

[40] S. Karataş " Effect of series resistance on the electrical characteristics and interface state energy distributions of Sn/p-Si (MS) Schottky diodes" Microelectron. Eng. **87** (2010) 1935-1940.

[41] W. Monch, Semiconductor Surfaces and Interfaces, third ed., Springer, Berlin, 2001.

[42] R. K Gupta, R. SA. Singh, "Electrical properties of junction between aluminium and poly(aniline)–poly(vinyl chloride) composite "Mater. Chem. Phys. **86** (2004) 279.

[43] S. Hardikar, M.K. Hudait, P. Modak, S.B. Krupanidhi, N. Padha, "Anomalous current transport in Au/low-doped n-GaAs Schottky barrier diodes at low temperatures" Appl. Phys. A **68** (1999) 49.

[44] R. D. Gould, M. S. Rahman, Organic Semiconductors, John Wiley, New York, 1967, pp. 359.

[45] R. D. Gould, "Annual survey of organometallic metal cluster chemistry for the year 1995" Coordin. Chem. Rev. **156** (1996) 237.

[46] J. G. Simmons, "Conduction in thin dielectric films "J. Phys. D: Appl. Phys. **4** (1971) 613-657.

[47] M. A. Green, "Solar Cells: Operating Principles, Technology and System Applications" University of New South Wales, Sydney, Australia, 1987, pp. 40 -169.

[48] A.A.M. Farag, E.A.A. El-Shazly, M. Abdel Rafea, A. Ibrahim " "Optical, electrical and photovoltaic characteristics of organic semiconductor based on oxazine/n-Si heterojunction" Sol. Energy Mater. Sol. Cells, **93** (10) (2009) 1853 – 1859.

Caption figures

Scheme1. Synthetic route for azochalcone derivative (**ACh**)

Scheme 2. Partial fragmentation of **ACh** compound.

Fig. 1. XRD patterns of **ACh** dye: (a) as-synthetized powder, (b) pristine film and (c) annealed film at 473 K for 2 hours.

Fig. 2. FE-SEM images of **ACh** dye: (a) the pristine film, (b) and (c) the annealed film with magnifications of 60 000 and 80 000, respectively.

Fig. 3. Optical absorption spectrum for the pristine and annealed **ACh** films.

Fig. 4. Optical transmittance and reflectance for the pristine and annealed **ACh** films.

Fig. 5. The spectral behavior of refractive index and extinction coefficient for the pristine and annealed **ACh** films.

Fig. 6: Variation of absorption coefficient, α, as a function of wavelength, λ.

Fig. 7: Plot of $(\alpha h\nu)^{1/2}$ as a function of the incident photon energy, $h\nu$, for the pristine and annealed **ACh** films.

Fig.8. Semi-log current-voltage characteristics of Au/**ACh**/p-Si/Al heterojunction solar cell in dark and under illumination conditions. The inset shows schematic diagram of the heterojunction solar cell.

Fig. 9. Plot of forward log I vs. log V for Au/**ACh**/p-Si/Al heterojunction solar cell.

Fig. 10. Plot of reverse log I_{rev} vs. $V^{1/2}$ for Au/**ACh**/p-Si/Al heterojunction solar cell.

Fig. 11. The power curve of Au/**ACh**/p-Si/Al heterojunction solar cell

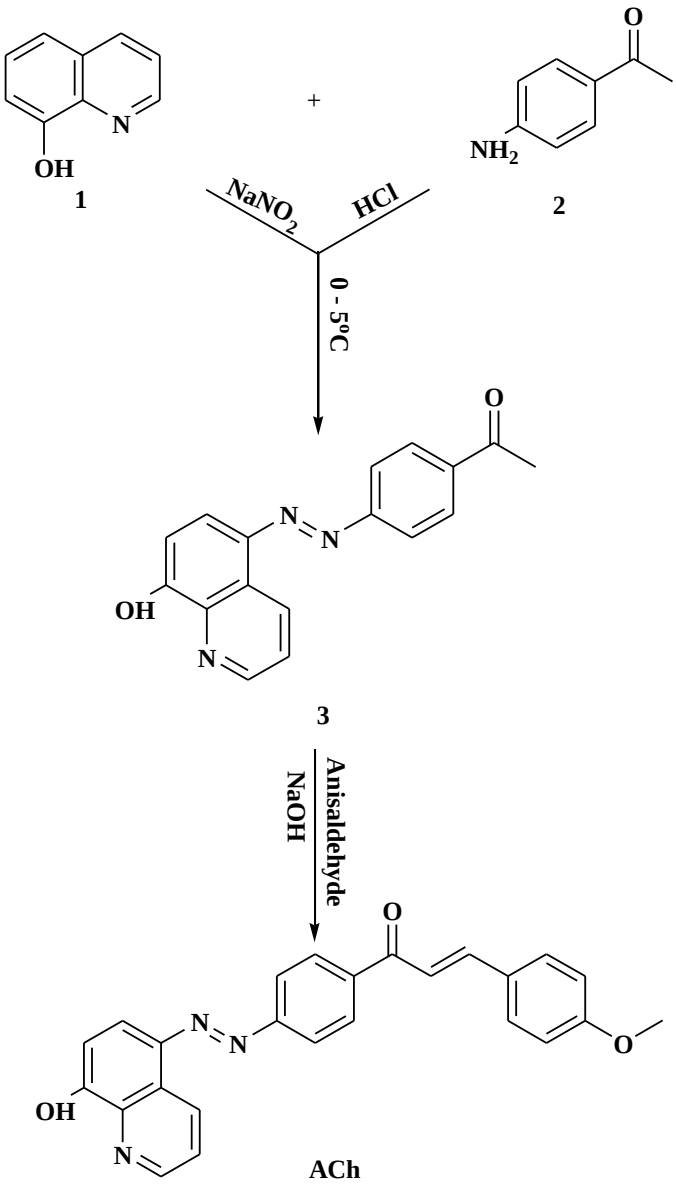

Scheme1

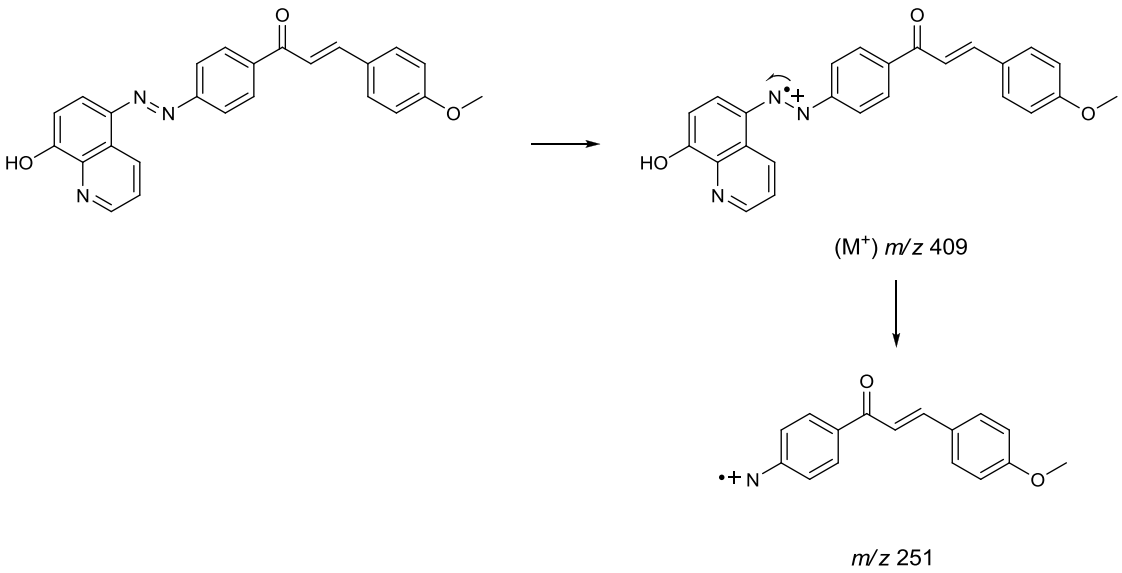

Scheme 2

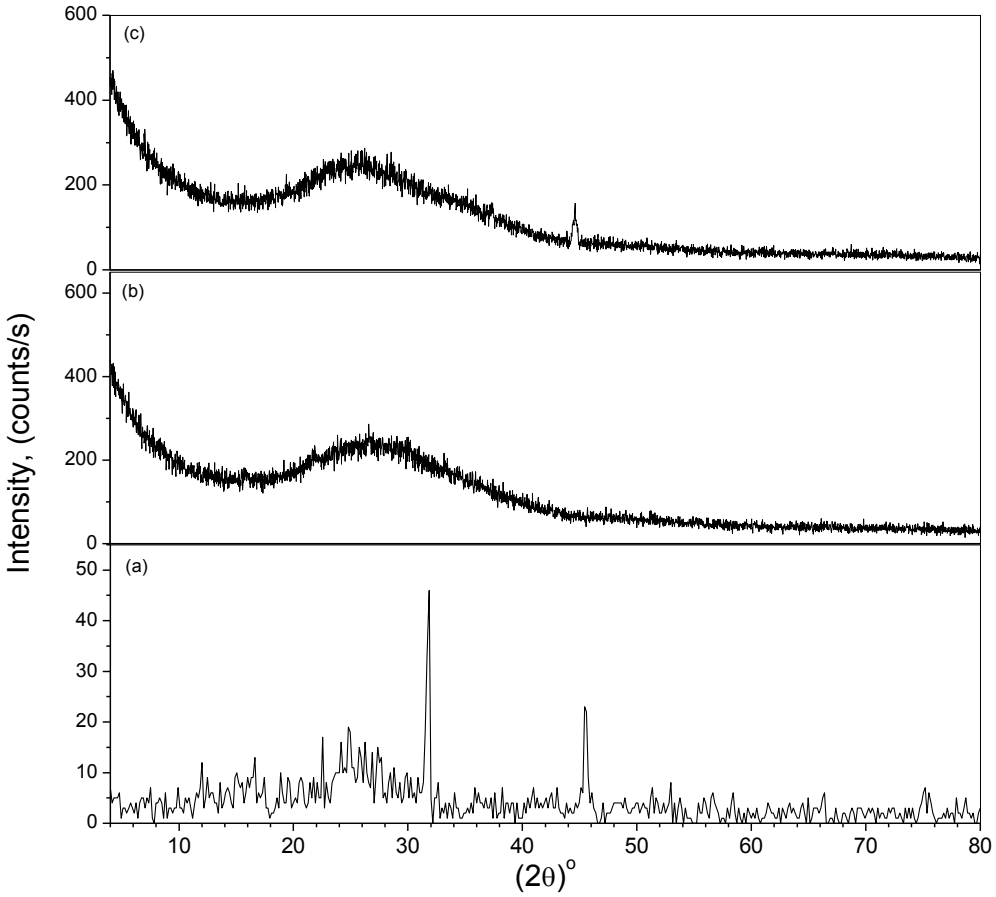

Fig. 1

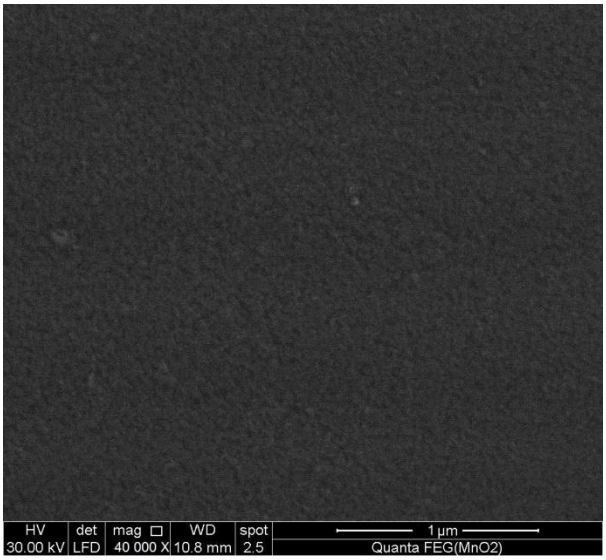

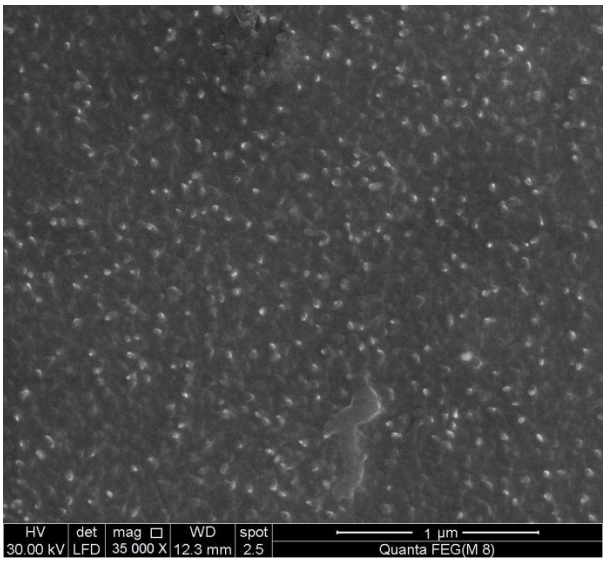

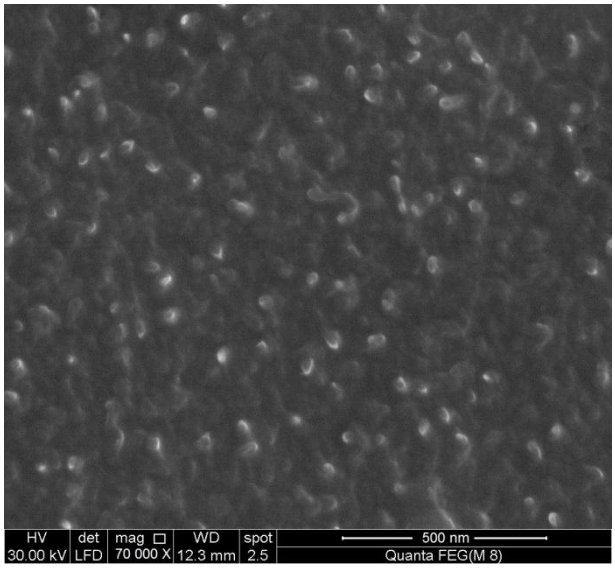

Fig. 2

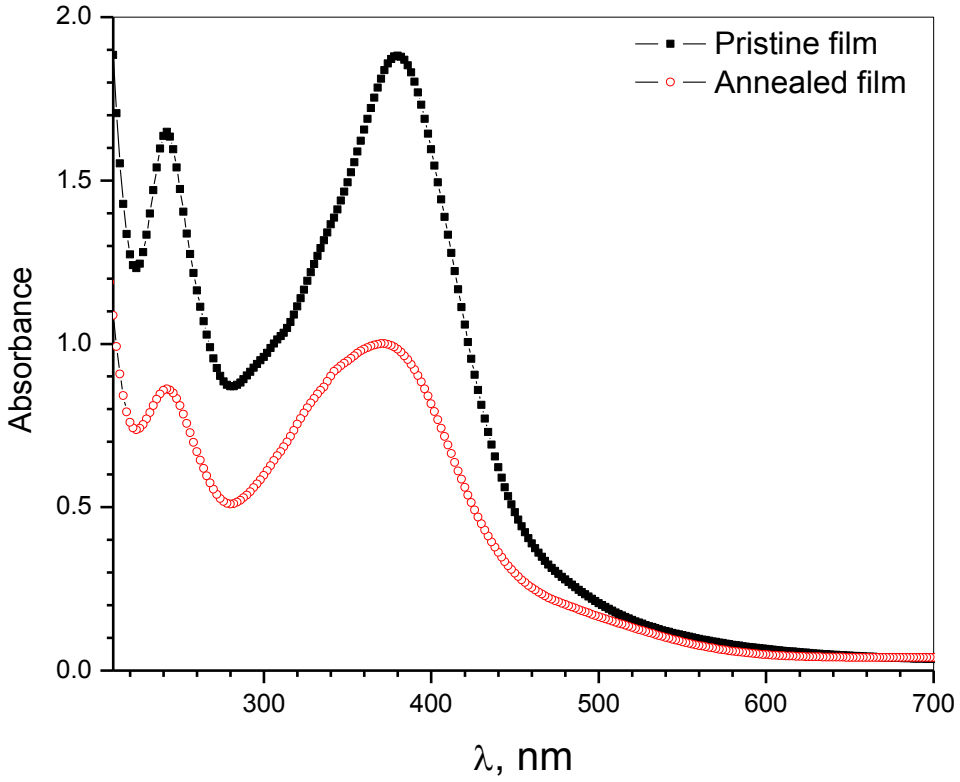

Fig. 3

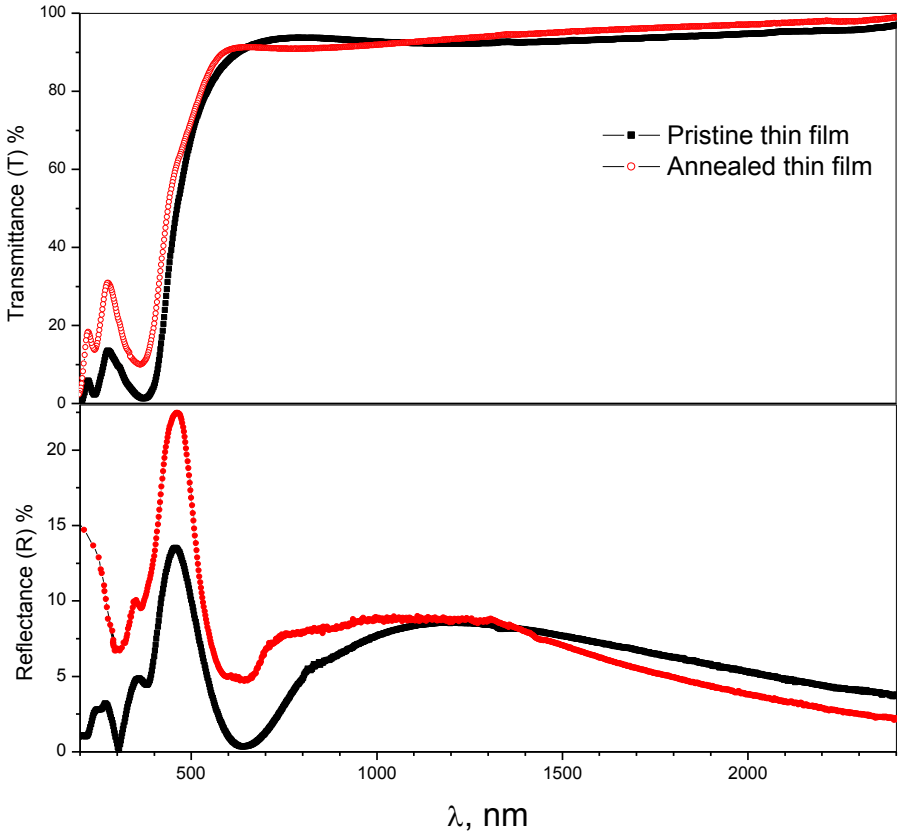

Fig. 4

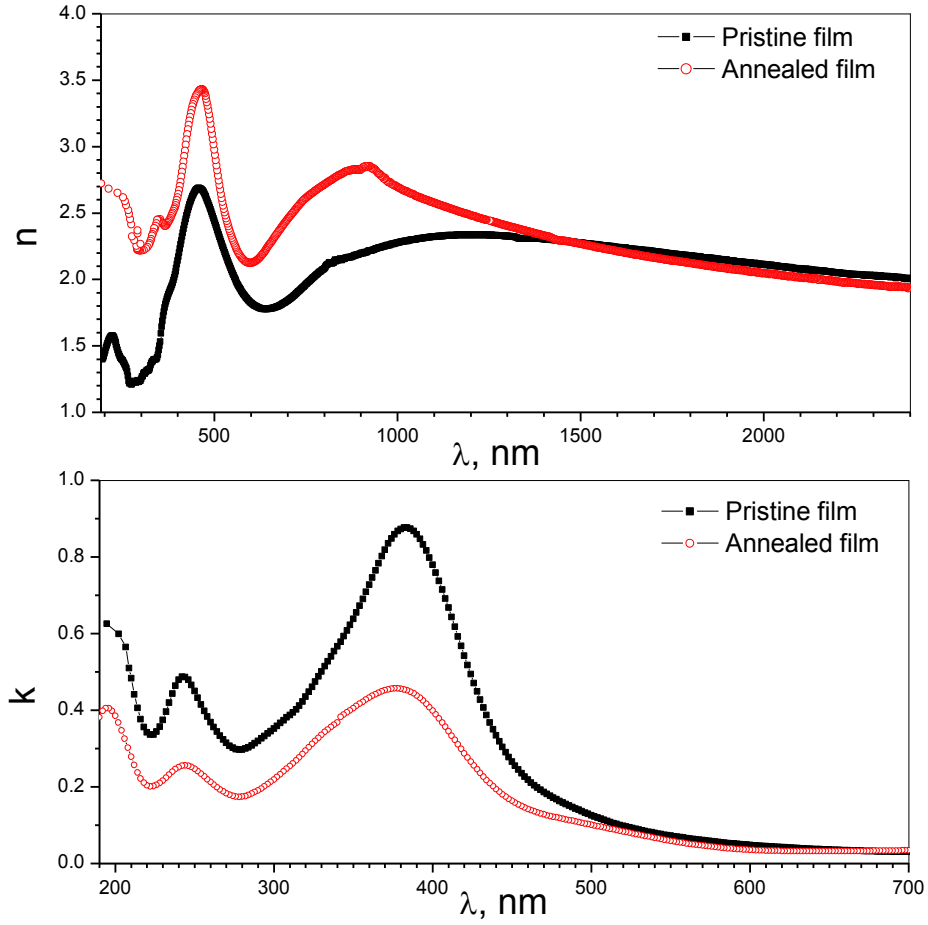

Fig. 5

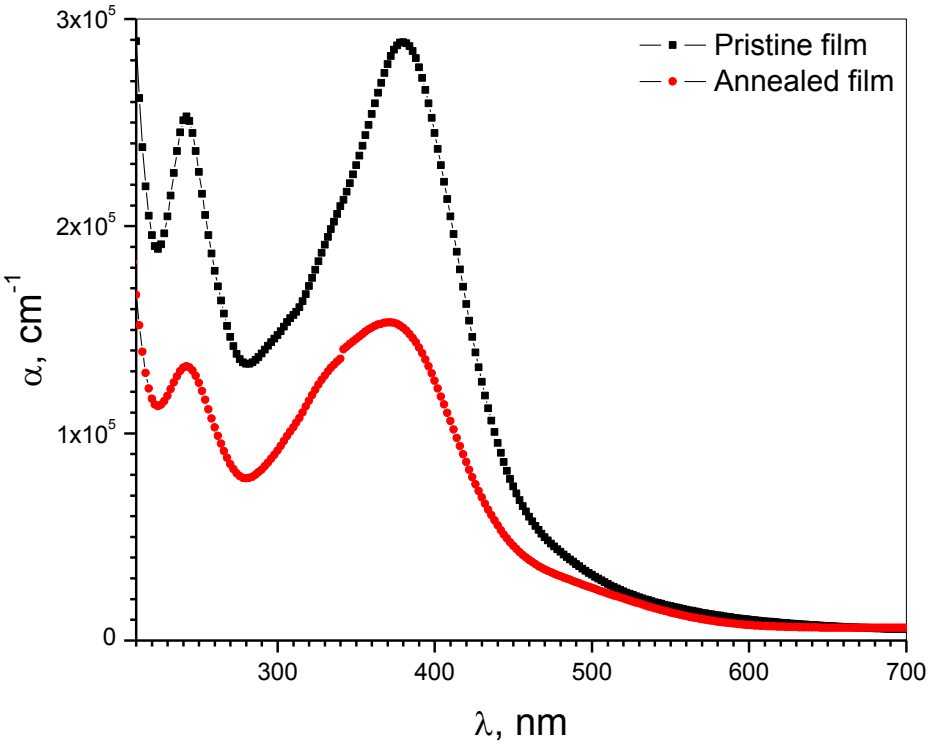

Fig. 6

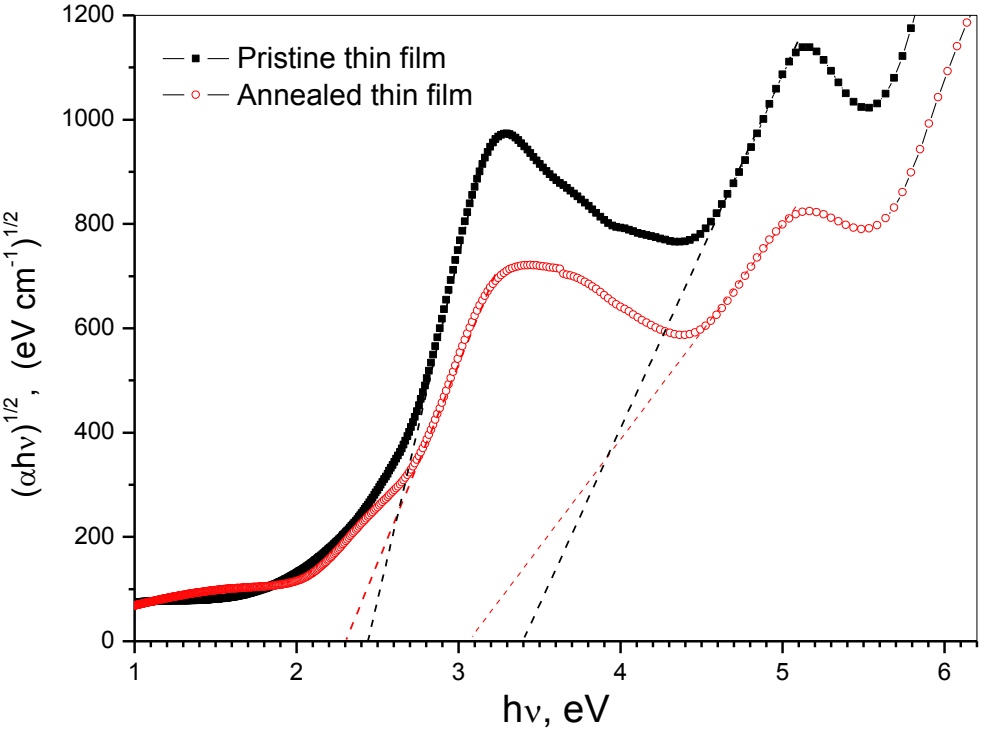

Fig. 7

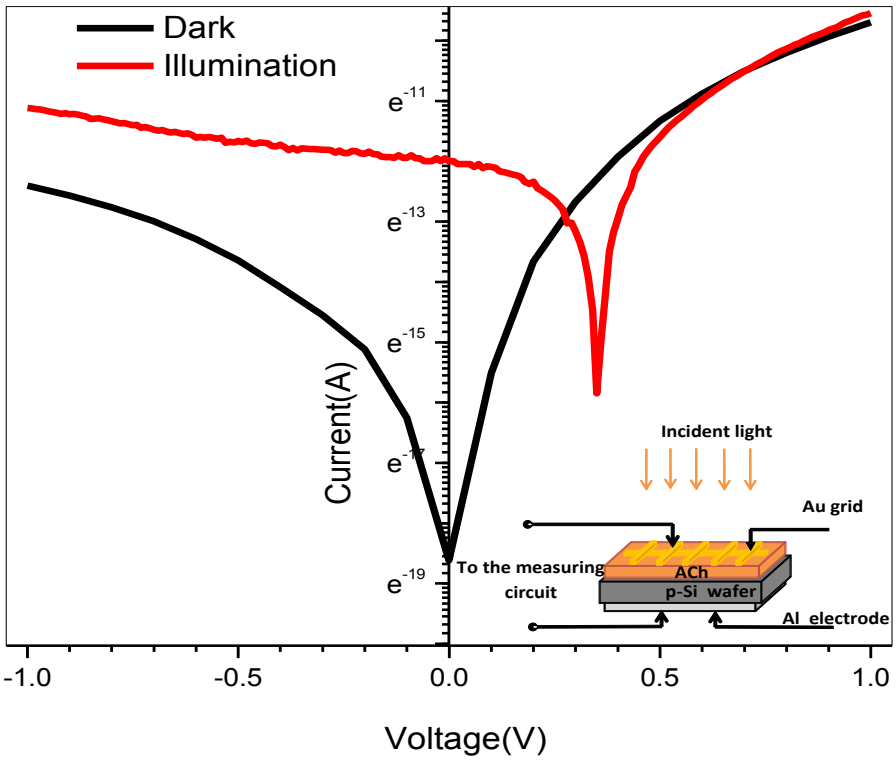

Fig. 8

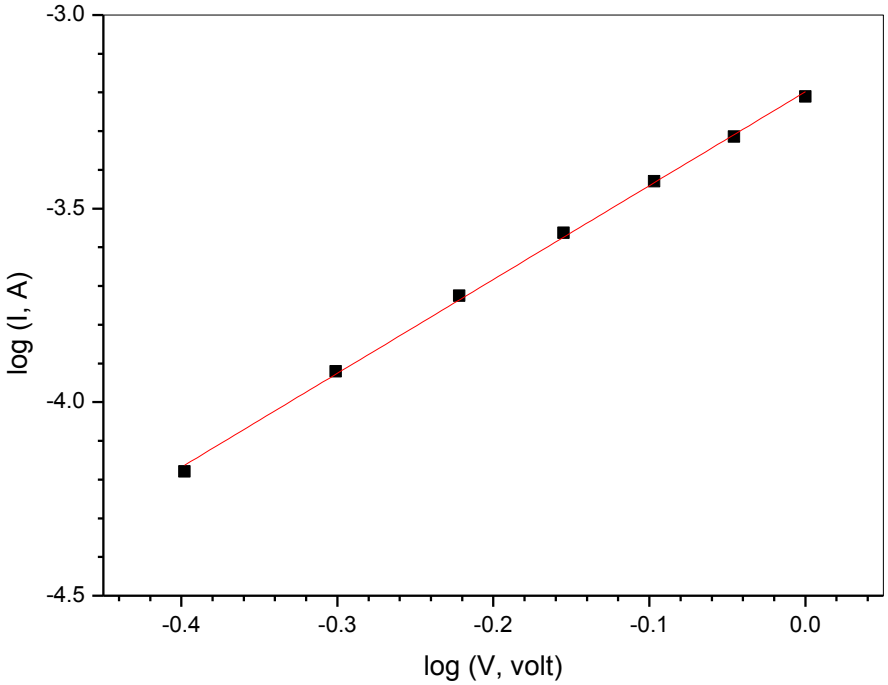

Fig. 9

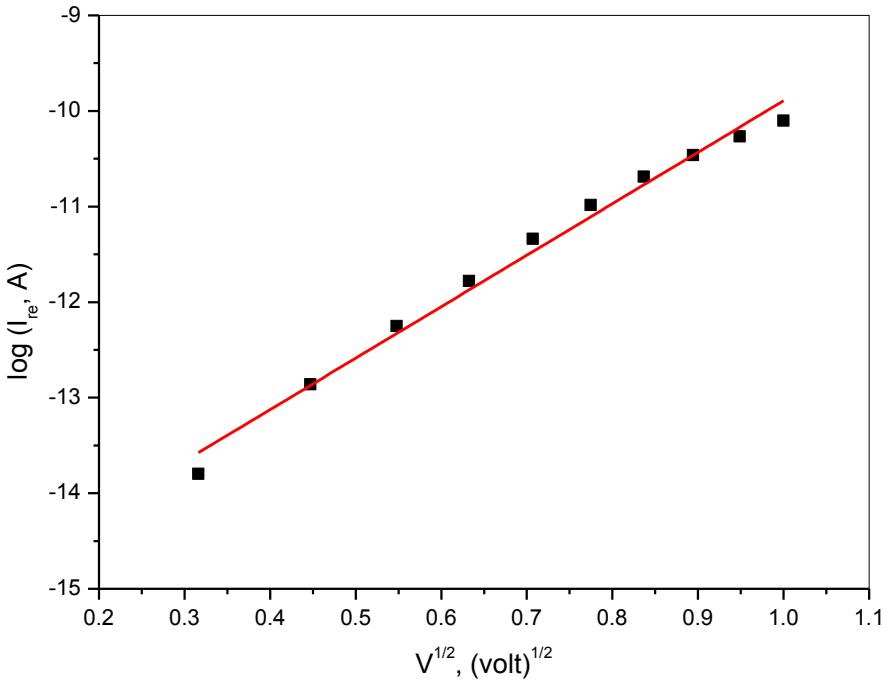

Fig. 10

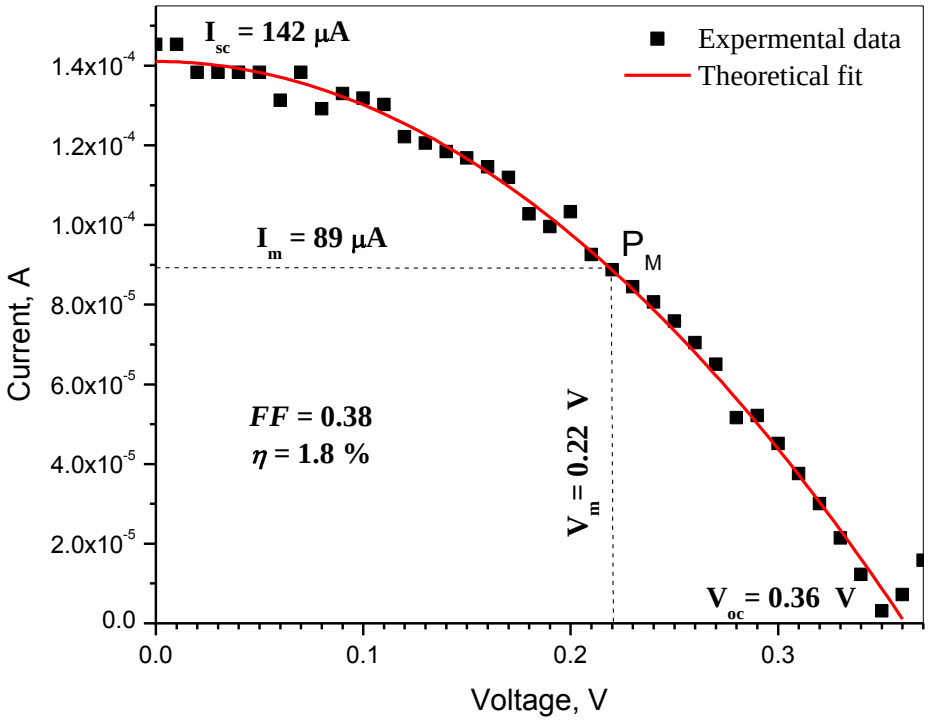

Fig. 11